#### **PAPER**

## Ultrafast bipolar conductivity driven by intense single-cycle terahertz pulses in a topological insulator Bi<sub>2</sub>Se<sub>3</sub>

To cite this article: L Luo et al 2021 J. Opt. 23 104003

View the article online for updates and enhancements.

#### You may also like

- Anisotropy in static and terahertz dynamic conductivities across in-plane axes of lanthanum nickel oxide thin films
  V Eswara Phanindra, K Santhosh Kumar and D S Rana
- Epitaxial strain driven crossover from Drude to Drude-Smith terahertz conductivity dynamics in LaNiO<sub>9</sub> thin films V Eswara Phanindra, Piyush Agarwal and D S Rana
- (Invited) Ultrafast Carrier Dynamics in Silicon Nanocrystal Films
  Lyubov V. Titova, Tyler L. Cocker, Xiongyao Wang et al.



### IOP ebooks™

Bringing together innovative digital publishing with leading authors from the global scientific community.

Start exploring the collection-download the first chapter of every title for free.

IOP Publishing Journal of Optics

J. Opt. 23 (2021) 104003 (6pp)

https://doi.org/10.1088/2040-8986/ac0316

# Ultrafast bipolar conductivity driven by intense single-cycle terahertz pulses in a topological insulator Bi<sub>2</sub>Se<sub>3</sub>

L Luo<sup>1</sup>, X Yang<sup>1</sup>, C Vaswani<sup>1</sup>, X Liu<sup>2</sup>, I E Perakis<sup>3</sup>, M Dobrowolska<sup>2</sup>, J K Furdyna<sup>2</sup> and J Wang<sup>1,\*</sup>

E-mail: jgwang@ameslab.gov

Received 15 January 2021, revised 3 May 2021 Accepted for publication 19 May 2021 Published 16 September 2021



#### **Abstract**

We present the measurement of ultrafast terahertz (THz) conductivity of a 50 nm thick topological insulator Bi<sub>2</sub>Se<sub>3</sub> at low temperature 5 K by using a THz pump and THz probe spectroscopy scheme. The THz conductivity driven by a single-cycle intense THz pump exhibits a bipolar lineshape and frequency-dependent relaxation dynamics due to the separated surface and bulk charge carriers with distinctly different scattering rates and relaxation times. We also demonstrate THz pump field-dependent excitation of the surface and bulk spectral weights, which suggests one of the optimal THz excitation conditions for generating the most charge carriers from the topology-protected surface state relative to the bulk. This also allows THz control of surface and bulk transport channels in a selective way.

Keywords: topological insulator, ultrafast terahertz conductivity, THz pump and THz probe spectroscopy

(Some figures may appear in colour only in the online journal)

#### 1. Introduction

Topological insulators are newly discovered quantum states of matter characterized by an insulating bandgap inside the bulk and a zero-gap conic band structure on the surface [1–6]. They exhibit many exotic quantum phenomena, such as strong spin-momentum locking and topology-protected charge transport in the surface, which prevent backscattering and result in very high carrier mobility and low energy consumption [7, 8]. These properties are highly desired for next-generation quantum computation and ultrafast spintronics applications with faster than THz speed [9–11].

THz conductivity of light-driven charge carriers in topological insulators by above-bandgap optical or below-bandgap mid-infrared (mid-IR) pulses have been studied [12–14]. Above-gap optical excitations induce interband charge transfer not only in the surface, but also in the high-density bulk reservoir dominantly, which can easily mask the topology-protected charge transport in the surface. In contrast, belowgap mid-IR pulses mostly excite intraband charge carriers of the surface and bulk near the Fermi energy  $E_{\rm F}$ , which is an excellent approach to significantly suppress unwanted interband charge transfer in the bulk reservoir and many other charge transfer channels [12]. This greatly helps disentangle the intrinsic topology-protected charge transport in the surface from the bulk conduction. It has been shown that topological insulator  $\rm Bi_2Se_3$  driven by below-gap mid-IR pulses at 5 K

<sup>&</sup>lt;sup>1</sup> Department of Physics and Astronomy and Ames Laboratory-U.S. DOE, Iowa State University, Ames, IA 50011, United States of America

<sup>&</sup>lt;sup>2</sup> Department of Physics, University of Notre Dame, Notre Dame, IN 46556, United States of America

<sup>&</sup>lt;sup>3</sup> Department of Physics, University of Alabama at Birmingham, Birmingham, AL 35294-1170, United States of America

<sup>\*</sup> Author to whom any correspondence should be addressed.

result in the change of scattering rates but conserved carrier densities of surface and bulk states, and the THz conductivity exhibits a bipolar lineshape and frequency-dependent carrier relaxation dynamics, due to the distinct charge carrier responses from separated surface and bulk states [12].

The next major opportunity is to investigate responses of THz conductivity driven by intense THz pulses, which carry a much lower photon energy than mid-IR pulses (a few meV vs. a couple of 100 meV), as a few meV THz photons are expected to favor surface excitation more than bulk, leading to greater spectral weight from surface carrier excitation [12]. To the best of our knowledge, THz conductivity of topological insulators driven by intense THz pulses has not been systematically studied so far and there has been only one set of such data available in literature that focuses on coherent  $E_{\rm u}$  phonon excitation [12, 15]. Especially, it is unclear whether the bipolar conductivity lineshape depends on THz pump strength, if THz-driven charge carriers exhibit frequency-dependent relaxation dynamics, and whether the spectral weight ratio of the surface and bulk can be tuned by THz pump strength.

In this article, we report a comprehensive study of singlecycle intense THz-driven THz conductivity in a 50 nm thick topological insulator Bi<sub>2</sub>Se<sub>3</sub> film using THz pump and THz probe (TPTP) spectroscopy scheme in transmission geometry [16-18]. We observe a bipolar lineshape of THz conductivity for both low and high THz pump fields up to 500 kV cm<sup>-1</sup>. The THz driven topological states indeed carries more spectral weight from the surface than that from mid-IR excitation. Moreover, the THz conductivity also exhibits frequency-dependent relaxation dynamics due to separated surface and bulk channels with different scattering rates and relaxation times. We also demonstrate that, by changing THz pump field strength, the spectral weight ratio of excited surface and bulk carriers can be tuned in a selective way, and the pump field at which the most surface carriers relative to bulk can be excited is found to be  $\sim$ 224 kV cm<sup>-1</sup>, suggesting one of the optimal THz excitation conditions in order to take advantage of topology-protected charge transport from the surface in optoelectronic applications. All analyses and conclusions in this study are made based on THz raw data without implications from any theoretical modeling or fitting.

#### 2. Experimental details

The sample we study is a 50 nm thin film of n-type  $Bi_2Se_3$  grown by molecular beam epitaxy on a 0.5 mm thick sapphire substrate. The Fermi energy  $E_F$  of the sample lies  $\sim$ 60 meV above the bulk conduction band edge as determined from the plasma frequency obtained from the static THz conductivity spectra [12, 15]. A pure sapphire substrate of the same thickness is used as a reference in order to extract THz conductivity of the  $Bi_2Se_3$  thin film. Both the sample and reference are mounted in a low temperature cryostat, and two copper apertures with a 2 mm diameter are placed in front of the sample and reference to ensure uniform illumination. All results presented in this study are measured at T=5 K.

Our single-cycle intense THz pulses, used as the pump (red lines in figure 1), are generated by optical rectification in a MgO doped LiNbO<sub>3</sub> crystal using the tilted pulse front method as shown in figure 1 [19, 20]. The LiNbO<sub>3</sub> crystal is pumped by a Ti:Sapphire regenerative amplifier with 790 nm central wavelength, 1 kHz repetition rate, 40 fs pulse duration, and 2 W power. The generated intense THz pulses have a peak field of  $\sim 1000 \text{ kV cm}^{-1}$  and a spectral bandwidth of  $\sim 1\text{--}10 \text{ meV}$ (0.24–2.42 THz). A representative pulse and its spectrum used in this study are shown in the inset of figure 2(a). The intense THz field strength is varied by a wire-grid polarizer (WGP1) in the beam in order to pump the sample with different field strength. The other part of the amplifier beam is used to generate (blue lines) and detect (green lines) the phase-locked THz probe field via optical rectification and electro-optic sampling in a 1 mm thick ZnTe crystal, respectively [21]. The THz probe has a spectral bandwidth of  $\sim$ 2–10.5 meV. The THz pump is vertically polarized and the THz probe is horizontally polarized. WGP2 serves as a beam combiner of pump and probe pulses. Both the THz pump and THz probe pulses are focused by a parabolic mirror with a 4-inch focal length at the sample position and their focal diameters are 1.2 mm and 0.8 mm, respectively. Afterwards, WGP3 transmits THz probe pulses and blocks THz pump pulses. The THz part of the setup is enclosed in a dry air purge box to reduce THz absorption by water vapor in air. A more detailed description of the setup can be found in [16].

In the measurement, THz probe field transmitted through the pure substrate  $E_{\text{ref}}(t_{\text{gate}})$  and unexcited sample  $E_{\text{sample}}(t_{\text{gate}})$ are measured by a gate (or sampling) pulse as a function of electro-optic sampling gate time  $t_{\text{gate}}$ . Pump-induced THz probe field changes  $\Delta E_{\text{sample}}(t_{\text{gate}})$  for various pump-probe time delay  $\Delta t_{pp}$  are also measured. Applying the fast Fourier transformation and Fresnel equations, static THz complex conductivity  $\tilde{\sigma}(\omega)$  and its pump induced change  $\Delta \tilde{\sigma}(\omega) =$  $\tilde{\sigma}^{\text{excited}}(\omega) - \tilde{\sigma}(\omega)$  are calculated as a function of probe photon energy  $\omega$ . The corresponding complex dielectric function  $\tilde{\varepsilon}(\omega)$  are calculated through  $\tilde{\sigma}(\omega) = i[1 - \tilde{\varepsilon}(\omega)]\omega\varepsilon_0$ . The real parts of the THz conductivity  $\sigma_1(\omega)$  and dielectric function  $\varepsilon_1(\omega)$  are presented in the study, which describe the dissipative and inductive responses of the sample, respectively. We note that although both THz pump and THz probe pulses are  $\sim 0.5$  ps long, the time resolution of the measurement is not determined by the pulse duration but rather on the order of the gate pulse width by the sampling of THz sub-cycles in the pump-probe  $\Delta t_{\rm pp}$  scan. Simply speaking, the gate pulse and pump pulse always sample the same probe pulse portion with the fixed  $\Delta t_{pp}$  even during the probe pulse duration. The measured THz probe field is the pump-induced change resolved during sub-cycle light oscillations, i.e.  $\Delta E_{\text{sample}}(t_{\text{gate}}) = E_{\text{excited-sample}}(t_{\text{gate}}) - E_{\text{sample}}(t_{\text{gate}})$ , as shown in figure 2(a). The pump-induced reshaping of the probe pulse will lead to nonzero  $\Delta E_{\text{sample}}$  signal even during the probe pulse duration because of the measuring probe E field sub-cycles not the pulse envelop only. Additional information about THz data analysis can be found in [12, 16, 22, 23].

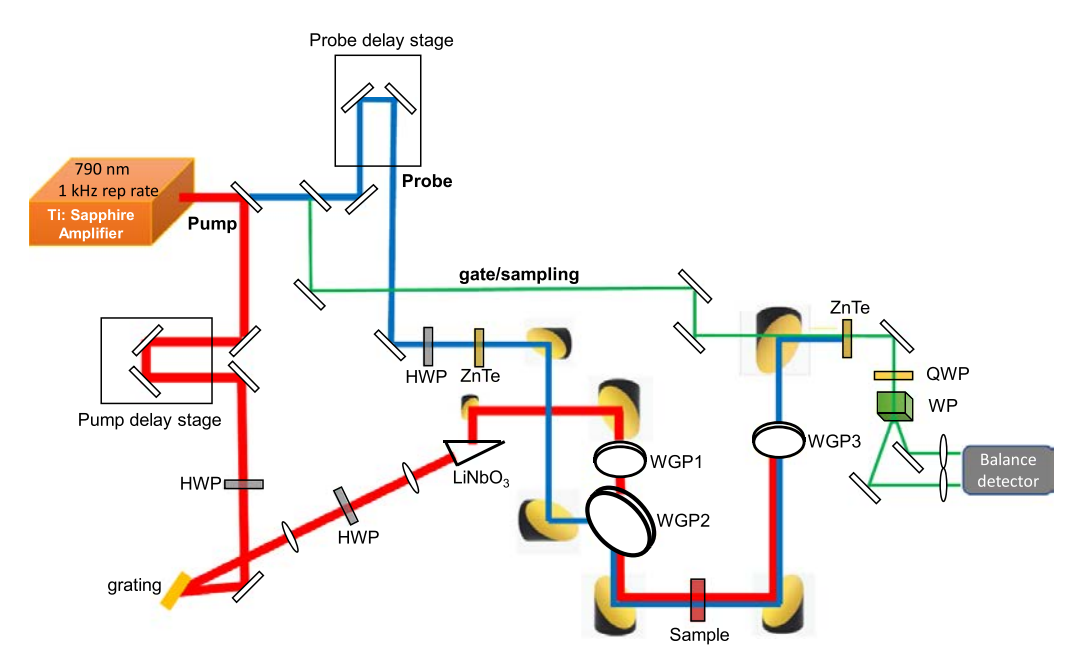


**Figure 1.** A schematic of THz pump and THz probe setup. The pump path is marked in red lines, the probe path is in blue lines, and the gate (or sampling) path is in green lines. HWP: half waveplate. WGP: wire grid polarizer. QWP: quarter waveplate. WP: wollaston prism.

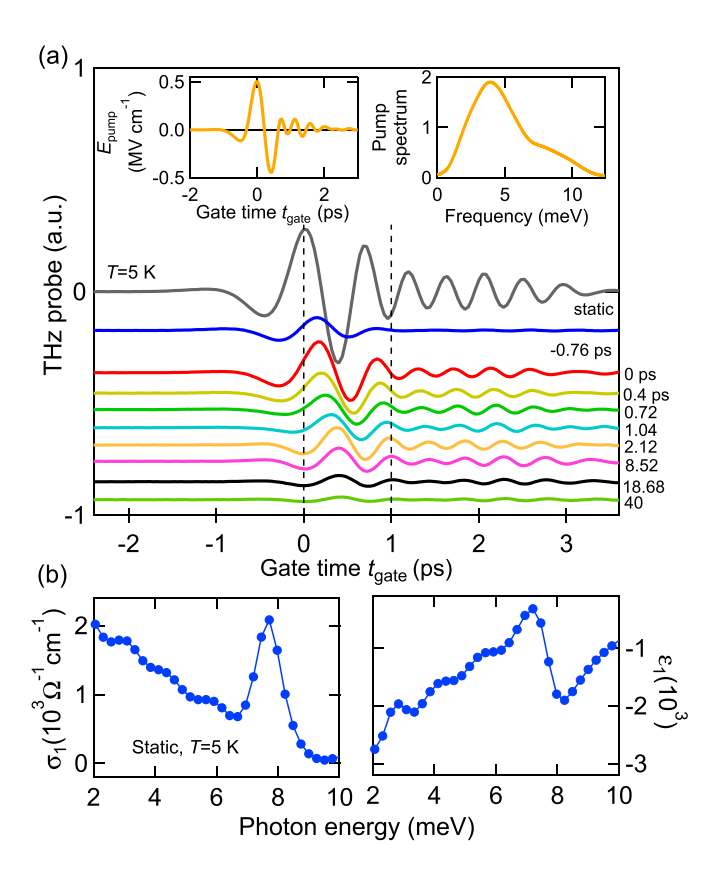


**Figure 2.** (a) Static THz probe signal  $E_{\text{sample}}(t_{\text{gate}})$  transmitted through the sample (gray curve) and its pump-induced changes  $\Delta E_{\text{sample}}(t_{\text{gate}})$  at various time delays (color curves) with a THz pump peak field  $E_{\text{pump}}$  of 500 kV cm $^{-1}$ , as shown in the insets in both time- and frequency-domains. The two vertical dashed lines are guides to the eyes. (b) Static THz conductivity  $\sigma_1(\omega)$  and dielectric function  $\varepsilon_1(\omega)$  of the sample.

#### 3. Experimental results and discussion

Figure 2(a) shows the static THz probe signal  $E_{\text{sample}}(t_{\text{gate}})$ after transmission through the sample (gray curve) and the pump-induced THz probe field changes  $\Delta E_{\text{sample}}(t_{\text{gate}})$  at various pump-probe time delays  $\Delta t_{\rm pp}$  (color curves) with a THz pump field of 500 kV cm<sup>-1</sup>, as shown in the inset. Besides an amplitude change, the pump-induced THz probe exhibits a phase shift with time, i.e. the field peak position gradually moves to the right as  $\Delta t_{\rm pp}$  increases. This feature is consistent with THz response following 248 meV mid-IR below-gap excitation at 5 K [12], which indicates more than one relaxation channel of excited charge carriers, discussed later. Static THz spectra of  $\sigma_1(\omega)$  and  $\varepsilon_1(\omega)$  are shown in figure 2(b), the lineshape of which is characterized by a Lorentzian oscillator centered at 7.7 meV originating from an optical phonon  $E_{\rm u}$ resonance and a Drude behavior originating from free charge carriers of both the surface and bulk states. These observations are fully consistent with prior measurements of static THz conductivity of Bi<sub>2</sub>Se<sub>3</sub> [15].

The pump-induced THz conductivity  $\Delta\sigma_1(\omega)$  and dielectric function  $\Delta\varepsilon_1(\omega)$  are presented in figures 3(a) and (b) for the pump field  $E_{\text{pump}}=500 \text{ kV cm}^{-1}$  and in figures 3(c) and (d) for a lower pump field  $E_{\text{pump}}=83 \text{ kV cm}^{-1}$ . They both exhibit a bipolar lineshape in the THz conductivity, i.e.  $\Delta\sigma_1(\omega)<0$  at lower  $\omega$  and  $\Delta\sigma_1(\omega)>0$  at higher  $\omega$ , at early time delays. After  $\sim 1 \text{ ps}$ ,  $\Delta\sigma_1(\omega)$  under the higher  $E_{\text{pump}}$  changes to mostly positive, as shown by the 1.04 ps case in figure 3(a). Afterwards,  $\Delta\sigma_1(\omega)$  is completely positive in the entire probe spectral range until it relaxes up to 40 ps. This lineshape of THz conductivity has been investigated by our prior study of below-gap mid-IR excitations at 5 K [12], from

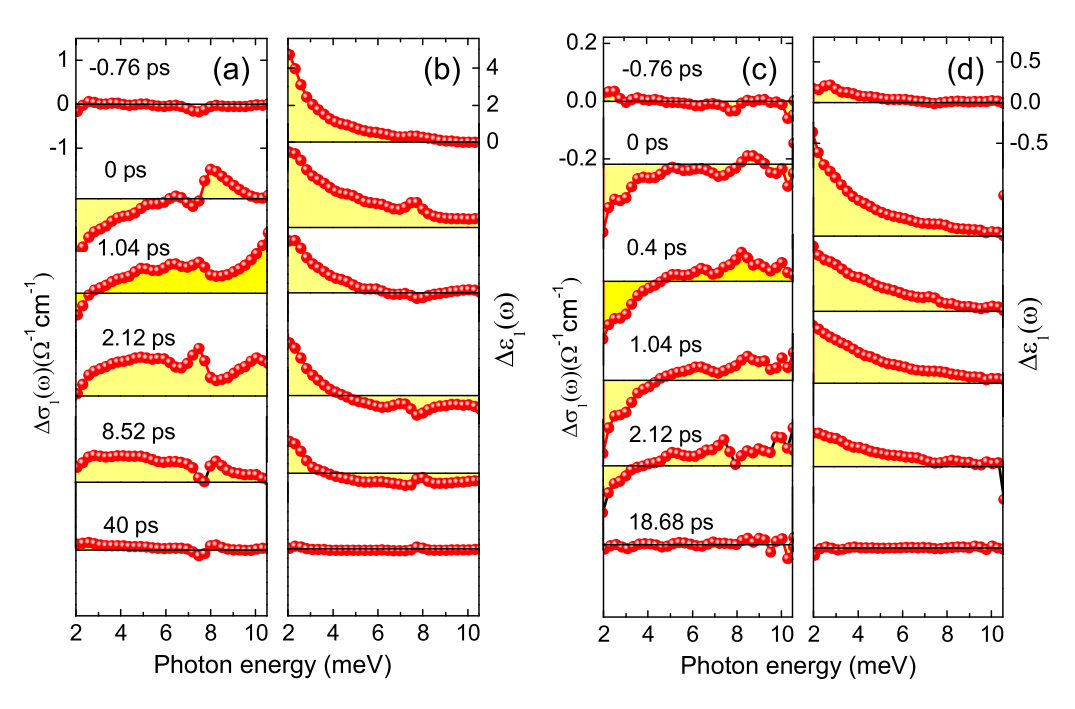


**Figure 3.** Pump-induced THz (a) conductivity  $\Delta \sigma_1(\omega)$  and (b) dielectric function  $\Delta \varepsilon_1(\omega)$  at various time delays with THz pump field of 500 kV cm<sup>-1</sup>. (c) and (d) Similar to (a) and (b), THz pump field is at 83 kV cm<sup>-1</sup> instead.

where the bipolar lineshape has been assigned mainly to the excited topology-protected charge carriers in the surface, due to photoexcited scattering rate increase and conserved carrier density. Because of the relatively faster relaxation time of surface carriers  $\sim 1.48$  ps compared to the bulk ones  $\sim 5.3$  ps [12], THz conductivity spectral weight from the surface is gradually diminished after a couple of ps. The THz responses at such a condition are dominated by the contribution from longer-lived bulk carriers, which is characterized by a positive conductivity similar to photoexcited normal semiconductors [22-25], as shown in figure 3(a) for  $\Delta t_{\rm pp} > 2$  ps. This scenario fully explains the observed THz conductivity driven by higher  $E_{pump}$  $= 500 \text{ kV cm}^{-1}$  in figure 3(a). More intriguingly, THz conductivity following the lower  $E_{\text{pump}} = 83 \text{ kV cm}^{-1}$  does not exhibit positive conductivity in the entire spectral range, indicating a surface-dominated spectral weight by lower THz pump excitation until it fully decays, as shown in figure 3(c). This comparison implies that a relatively lower  $E_{pump}$  can excite more surface carriers relative to the bulk. However  $E_{\mathrm{pump}}$  cannot be too small, in which case the excited surface transport may otherwise be too weak to probe. A more detailed THz pump field-dependent measurement will be presented later in figure 5. A detailed discussion of the phonon dynamics centered at 7.7 meV has been reported in [12, 15].

Protected by topology, the scattering rate of carriers in the surface is expected to be much smaller than that in the bulk, as confirmed by the prior mid-IR pumping experiment [12]. This, together with distinct relaxation dynamics of surface and bulk carriers as discussed in figure 3, suggests two distinct charge relaxation channels and frequency-dependent THz conductivity relaxation dynamics. This argument is further verified in figure 4, which shows  $\Delta \sigma_1(\omega)$  and  $\Delta \varepsilon_1(\omega)$  from five frequency-cut positions from figure 3, i.e.  $\omega=2$ ,

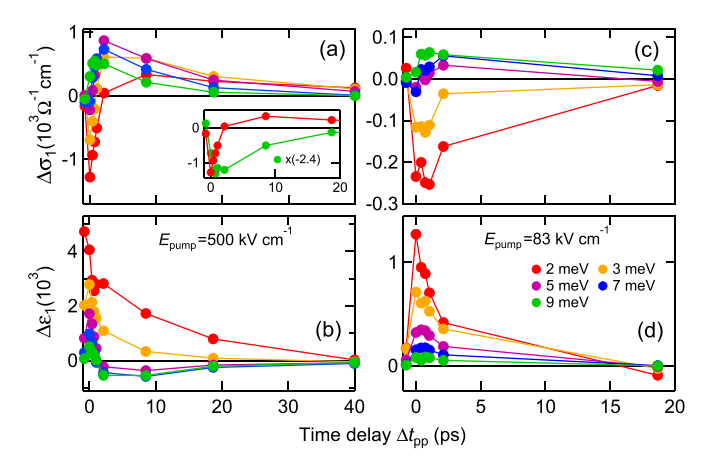


**Figure 4.** Pump-induced (a) THz conductivity  $\Delta\sigma_1(\omega)$  and (b) dielectric function  $\Delta\varepsilon_1(\omega)$  at five frequency-cut positions from figures 3(a) and (b), respectively, i.e. at  $\omega=2,3,5,7,9$  meV, as a function of time delay and with  $E_{\rm pump}=500~{\rm kV~cm}^{-1}$ . The inset of (a) exclusively compares  $\Delta\sigma_1(\omega)$  dynamics at  $\omega=2$  and 9 meV (9 meV data is multiplied by -2.4 to match their amplitudes) to show their distinct relaxation times. The units of the inset are the same as (a). (c) and (d) similar to (a) and (b), they are from figures 3(c) and (d), respectively, and with  $E_{\rm pump}=83~{\rm kV~cm}^{-1}$ .

3, 5, 7, 9 meV, as a function of time delay. They clearly exhibit different relaxation behaviors at different probe frequency for both higher and lower  $E_{\text{pump}}$ . For a better illustration,  $\Delta\sigma_1(\omega)$  for  $\omega=2$  and 9 meV from figure 4(a) are compared exclusively ( $\Delta\sigma_1(\omega)$  at  $\omega=9$  meV is normalized to the other by multiplying -2.4), as shown in the inset of figure 4(a), in which  $\Delta\sigma_1(\omega)$  at  $\omega=2$  meV (red dots) decays much faster than  $\Delta\sigma_1(\omega)$  at  $\omega=9$  meV (green dots). Apparently, the relaxation time depends on the probe frequency,

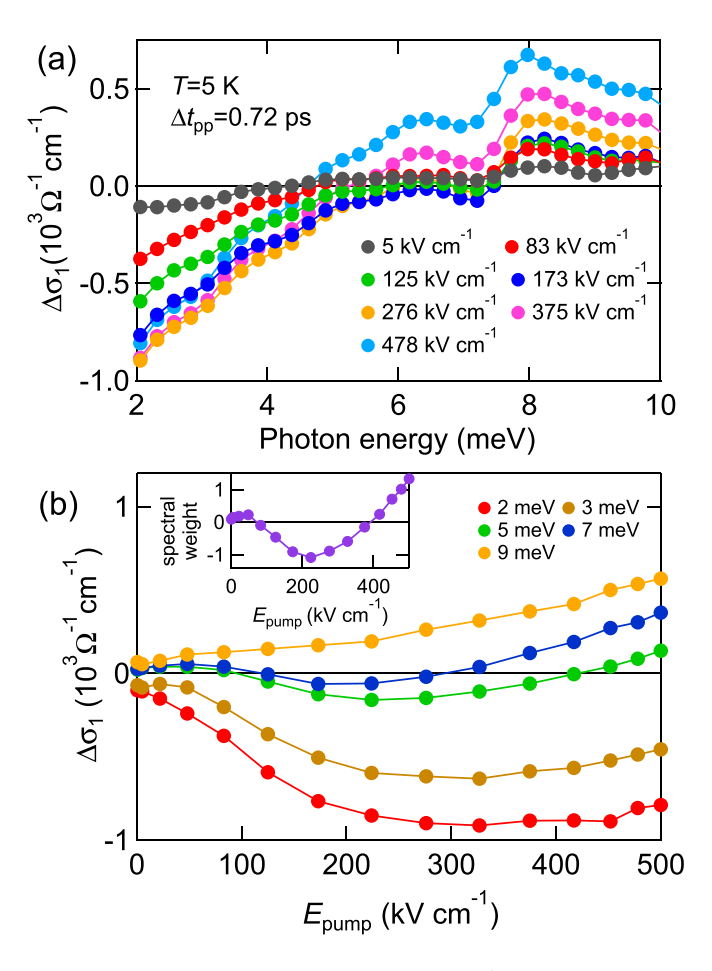


**Figure 5.** (a) Pump-induced THz conductivity  $\Delta\sigma_1(\omega)$  at various pump fields and  $\Delta t_{\rm pp}=0.72$  ps. (b) Pump-induced THz conductivity  $\Delta\sigma_1(\omega)$  at five frequency-cut positions from (a), i.e. at  $\omega=2,3,5,7,9$  meV, as a function of  $E_{\rm pump}$  from 5 to 500 kV cm<sup>-1</sup>. The inset plots the integrated spectral weight of conductivity, i.e.  $\int_{2\,{\rm meV}}^{10\,{\rm meV}} \Delta\sigma_1(\omega)\,{\rm d}\omega$  from figure 5(a), as a function of  $E_{\rm pump}$ .

and the faster (slower) relaxation is mainly from the surface (bulk) states, fully consistent with THz conductivity dynamics driven by mid-IR pulses [12]. Figure 4 also corroborates observations discussed in figure 3 that THz conductivity is positive for all probe frequencies up to 40 ps for the higher  $E_{\text{pump}}$  (figure 4(a)) indicating a bulk dominated THz response and spectral weight; while it remains a bipolar lineshape up to  $\sim$ 20 ps for the lower  $E_{\text{pump}}$  (figure 4(c)) indicating a surface dominated THz response and spectral weight. Please refer to our prior study if one is interested in detailed theoretical fitting and modeling of the surface and bulk relaxation dynamics by below-gap excitation [12].

To investigate how THz pump strength may control excitations of surface and bulk carriers respectively, and if so, how much pump strength can result in the maximum surface excitation relative to bulk, figure 5(a) presents pump field-dependent THz conductivity  $\Delta\sigma_1(\omega)$  at a delay time  $\Delta t_{\rm pp}=0.72$  ps. This delay time is chosen because it is right after the excitation of the sample by the THz pump main peak (inset of figure 2(a)), so that spectral weight with genuine population ratio of surface and bulk carriers can be probed immediately, before the relatively faster relaxation of surface carriers within

a couple of ps. Figure 5(b) plots  $\Delta \sigma_1(\omega)$  at several frequencycut positions, i.e.  $\omega = 2, 3, 5, 7, 9$  meV, from figure 5(a) as a function of  $E_{\text{pump}}$ . As  $E_{\text{pump}}$  increases,  $\Delta \sigma_1(\omega)$  in general changes to more negative amplitude until  $\sim$ 200–300 kV cm<sup>-1</sup>. Afterwards, it changes towards positive amplitude for all frequencies. To better illustrate the pump field-dependent behavior, the spectral weight of  $\Delta \sigma_1(\omega)$  from 2 to 10 meV, i.e.  $\int_{2\mathrm{meV}}^{10\mathrm{meV}} \Delta\sigma_1(\omega)\,\mathrm{d}\omega,$  as a function of THz pump field is summarized in the inset, which indeed follows a similar trend as observed in figure 5(b). It initially increases towards negative amplitude and reaches the negative maximum at  $E_{pump} = 224$ kV cm<sup>-1</sup> implying the greatest surface carrier excitation relative to the bulk. Further increasing the pump field decreases this ratio, and above  $\sim$ 420 kV cm<sup>-1</sup> the spectral weight changes to positive, indicating more quickly growing of bulk excitation over the surface at higher pump field. This finding allows the THz control of surface and bulk transport channels in a selective way. We expect that the bipolar lineshape will change to completely positive at a much higher  $E_{pump}$ , which indicates the dominant spectral weight from the bulk state instead of the surface.

#### 4. Conclusion

In conclusion, we have provided a comprehensive measurement of single-cycle intense THz pulse-induced conductivity of a topological insulator Bi<sub>2</sub>Se<sub>3</sub> at low temperature 5 K by using THz pump and THz probe spectroscopy. The ultrafast THz conductivity spectra exhibit a bipolar lineshape up to 500 kV cm<sup>-1</sup> pump field. It also exhibits frequency-dependent relaxation dynamics, due to separated surface and bulk transport channels with distinct scattering rate and relaxation time. The THz responses driven by intense THz pulses confirm the non-equilibrium dynamics driven by below-gap excitations, e.g. using mid-IR pulses. Most importantly, we have demonstrated a new tuning knob for controlling spectral weight ratio of excited surface and bulk charge carriers by changing THz pump field strength. All analyses and statements in this study are made based on THz raw data without implications and uncertainties from any theoretical modeling or fitting. The single-cycle THz excitation and spectroscopy may be extended to diverse complex materials including magnets [26–29] and correlated electrons [30-33]. Our findings also provide previously-inaccessible, key information for exploring both fundamental topological quantum phenomena and technological applications involving THz single-cycle excitations.

#### Data availability statement

The data generated and/or analysed during the current study is not publicly available for legal/ethical reasons but are available from the corresponding author on reasonable request.

#### **Acknowledgment**

This work was supported by the U.S. Department of Energy, Office of Basic Energy Science, Division of Materials J. Opt. 23 (2021) 104003 L Luo et al

Sciences and Engineering (Ames Laboratory is operated for the U.S. Department of Energy by Iowa State University under Contract No. DE-AC02-07CH11358). Sample development was supported by National Science Foundation DMR 1400432. I E P at the University of Alabama, Birmingham, was supported by the US Department of Energy, Office of Science, Basic Energy Sciences, under Award No. DE-SC0019137.

#### **ORCID iDs**

X Yang https://orcid.org/0000-0002-3856-8182 J Wang https://orcid.org/0000-0002-6159-4119

#### References

- [1] Moore J E 2010 The birth of topological insulators *Nature* 464 194–8
- [2] Hasan M Z and Kane C L 2010 Colloquium: topological insulators Rev. Mod. Phys. 82 3045–67
- [3] Fu L and Kane C L 2007 Topological insulators with inversion symmetry *Phys. Rev.* B 76 045302
- [4] Hsieh D et al 2009 A tunable topological insulator in the spin helical Dirac transport regime Nature 460 1101–5
- [5] Vaswani C et al 2020 Light-driven Raman coherence as a nonthermal route to ultrafast topology switching in a Dirac semimetal Phys. Rev. X 10 021013
- [6] Luo L et al 2020 A light-induced phononic symmetry switch and giant dissipationless topological photocurrent in ZrTe<sub>5</sub> Nat. Mater. 20 329
- [7] Rachel S 2018 Interacting topological insulators: a review Rep. Prog. Phys. 81 116501
- [8] Hasan M Z and Moore J E 2011 Three-dimensional topological insulators *Annu. Rev. Condens. Matter Phys.* 2 55–78
- [9] He M, Sun H and He Q L 2019 Topological insulator: spintronics and quantum computations *Front. Phys.* 14 43401
- [10] Wang M C, Qiao S, Jiang Z, Luo S N and Qi J 2016 Unraveling photoinduced spin dynamics in the topological insulator Bi<sub>2</sub>Se<sub>3</sub> Phys. Rev. Lett. 116 036601
- [11] Kim R H et al 2021 Terahertz Nano-Imaging of Electronic Strip Heterogeneity in a Dirac Semimetal Terahertz Nano-Imaging of Electronic Strip Heterogeneity in a Dirac Semimetal ACS Photonics 8 1873–80
- [12] Luo L *et al* 2019 Ultrafast manipulation of topologically enhanced surface transport driven by mid-infrared and terahertz pulses in Bi<sub>2</sub>Se<sub>3</sub> *Nat. Commun.*
- [13] Sim S, Brahlek M, Koirala N, Cha S, Oh S and Choi H 2014 Ultrafast terahertz dynamics of hot Dirac-electron surface scattering in the topological insulator Bi<sub>2</sub>Se<sub>3</sub> *Phys. Rev.* B 89 165137
- [14] Aguilar R V et al 2015 Time-resolved terahertz dynamics in thin films of the topological insulator Bi<sub>2</sub>Se<sub>3</sub> Appl. Phys. Lett. 106 011901
- [15] Yang X et al 2020 Light control of surface–bulk coupling by terahertz vibrational coherence in a topological insulator npj Quantum Mater. 5 13

[16] Yang X et al 2018 Terahertz-light quantum tuning of a metastable emergent phase hidden by superconductivity Nat. Mater. 17 586–91

- [17] Yang X et al 2019 Lightwave-driven gapless superconductivity and forbidden quantum beats by terahertz symmetry breaking Nat. Photon. 13 707–13
- [18] Vaswani C et al 2020 Terahertz second-harmonic generation from lightwave acceleration of symmetry-breaking nonlinear supercurrents Phys. Rev. Lett. 124 207003
- [19] Liu Z et al 2020 Ultrafast control of excitonic rashba fine structure by phonon coherence in the metal halide perovskite CH<sub>3</sub>NH<sub>3</sub>PbI<sub>3</sub> Phys. Rev. Lett. 124 157401
- [20] Liu Z et al 2020 Coherent band-edge oscillations and dynamic longitudinal-optical phonon mode splitting as evidence for polarons in perovskites Phys. Rev. B 101 115125
- [21] Luo L, Chatzakis I, Wang J, Niesler F B P, Wegener M, Koschny T and Soukoulis C M 2014 Broadband terahertz generation from metamaterials *Nat. Commun.* 5 3055
- [22] Luo L et al 2017 Ultrafast terahertz snapshots of excitonic Rydberg states and electronic coherence in an organometal halide perovskite Nat. Commun. 8 15565
- [23] Luo L, Chatzakis I, Patz A and Wang J 2015 Ultrafast terahertz probes of interacting dark excitons in chirality-specific semiconducting single-walled carbon nanotubes *Phys. Rev. Lett.* 114 107402
- [24] Luo L, Liu Z, Yang X, Vaswani C, Cheng D, Park J-M and Wang J 2019 Anomalous variations of spectral linewidth in internal excitonic quantum transitions of ultrafast resonantly excited single-walled carbon nanotubes *Phys. Rev. Mater.* 3 026003
- [25] Chatzakis I, Luo L, Wang J, Shen N-H, Koschny T, Zhou J and Soukoulis C M 2012 Reversible modulation and ultrafast dynamics of terahertz resonances in strongly photoexcited metamaterials *Phys. Rev.* B 86 125110
- [26] Patz A, Li T, Ran S, Fernandes R M, Schmalian J, Bud'ko S L, Canfield P C, Perakis I E and Wang J 2014 Ultrafast observation of critical nematic fluctuations and giant magnetoelastic coupling in iron pnictides *Nat. Commun.* 5 3229
- [27] Patz A, Li T, Liu X, Furdyna J K, Perakis I E and Wang J 2015 Ultrafast probes of nonequilibrium hole spin relaxation in the ferromagnetic semiconductor GaMnAs *Phys. Rev.* B 91 155108
- [28] Wang J, Khodaparast G A, Kono J, Slupinski T, Oiwa A and Munekata H 2004 Ultrafast softening in InMnAs *Physica* E 20 412–18
- [29] Patz A et al 2014 Ultrafast observation of critical nematic fluctuations and giant magnetoelastic coupling in iron pnictides Nat. Commun. 5 3229
- [30] Patz A, Li T, Luo L, Yang X, Bud'ko S, Canfield P C, Perakis I E and Wang J 2017 Critical speeding up of nonequilibrium electronic relaxation near nematic phase transition in unstrained Ba(Fe<sub>1-x</sub>Co<sub>x</sub>)<sub>2</sub>As<sub>2</sub> *Phys. Rev.* B **95** 165122
- [31] Yang X et al 2018 Ultrafast nonthermal terahertz electrodynamics and possible quantum energy transfer in the Nb<sub>3</sub>Sn superconductor *Phys. Rev.* B **99** 094504
- [32] Vaswani C *et al* 2020 Light quantum control of persisting Higgs modes in iron-based superconductors *Nat. Commun.* 12 258
- [33] Li T, Patz A, Mouchliadis L, Yan J, Lograsso T A, Perakis I E and Wang J 2013 Femtosecond switching of magnetism via strongly correlated spin–charge quantum excitations *Nature* 496 69